

A VLA Survey of Late-time Radio Emission from Superluminous Supernovae and the Host Galaxies

BUNYO HATSUKADE ¹, NOZOMU TOMINAGA ^{2,3,4}, TOMOKI MOROKUMA ¹, KANA MOROKUMA-MATSUI ¹,
YUICHI MATSUDA ^{2,5}, YOICHI TAMURA ⁶, KOTARO NIINUMA ⁷ AND KAZUHIRO MOTOGI ⁷

¹*Institute of Astronomy, Graduate School of Science, The University of Tokyo, 2-21-1 Osawa, Mitaka, Tokyo 181-0015, Japan*

²*National Astronomical Observatory of Japan, 2-21-1 Osawa, Mitaka, Tokyo 181-8588, Japan*

³*Department of Physics, Faculty of Science and Engineering, Konan University, 8-9-1 Okamoto, Kobe, Hyogo 658-8501, Japan*

⁴*Kavli Institute for the Physics and Mathematics of the Universe (WPI), The University of Tokyo, 5-1-5 Kashiwanoha, Kashiwa, Chiba 277-8583, Japan*

⁵*Graduate University for Advanced Studies (SOKENDAI), Osawa 2-21-1, Mitaka, Tokyo 181-8588, Japan*

⁶*Department of Physics, Nagoya University, Furo-cho, Chikusa-ku, Nagoya 464-8602, Japan*

⁷*Graduate School of Sciences and Technology for Innovation, Yamaguchi University, Yoshida 1677-1, Yamaguchi, Yamaguchi 753-8512, Japan*

(Received June 25, 2021; Revised August 12, 2021; Accepted August 23, 2021)

ABSTRACT

We present the results of 3 GHz radio continuum observations of 23 superluminous supernovae (SLSNe) and their host galaxies by using the Karl G. Jansky Very Large Array conducted 5–21 years after the explosions. The sample consists of 15 Type I and 8 Type II SLSNe at $z < 0.3$, providing one of the largest sample of SLSNe with late-time radio data. We detected radio emission from one SLSN (PTF10hgi) and 5 hosts with a significance of $>5\sigma$. No time variability is found in late-time radio light curves of the radio-detected sources in a timescale of years except for PTF10hgi, whose variability is reported in a separate study. Comparison of star-formation rates (SFRs) derived from the 3 GHz flux densities with those derived from SED modeling based on UV–NIR data shows that four hosts have an excess of radio SFRs, suggesting obscured star formation. Upper limits for undetected hosts and stacked results show that the majority of the SLSN hosts do not have a significant obscured star formation. By using the 3 GHz upper limits, we constrain the parameters for afterglows arising from interaction between initially off-axis jets and circumstellar medium (CSM). We found that the models with higher energies ($E_{\text{iso}} \gtrsim \text{several} \times 10^{53}$ erg) and CSM densities ($n \gtrsim 0.01 \text{ cm}^{-3}$) are excluded, but lower energies or CSM densities are not excluded with the current data. We also constrained the models of pulsar wind nebulae powered by a newly born magnetar for a subsample of SLSNe with model predictions in the literature.

Keywords: Radio transient sources (2008); Extragalactic radio sources (508); Supernovae (1668); Circumstellar matter (241); Radio continuum emission (1340); Very Large Array (1766); Radio Astronomy (1338)

1. INTRODUCTION

Superluminous supernovae (SLSNe) are very bright explosions (>10 – 100 times brighter) and rare events (<100 times lower) compared to ordinary SNe (Gal-Yam 2012, 2019; Moriya et al. 2018, for reviews). SLSNe are detected at high redshifts up to $z \sim 4$ (Cooke et al.

2012; Moriya et al. 2019), and therefore can be powerful probes of the distant universe. The power source and mechanism for large luminosities are still a matter of debate. SLSNe are classified into two types according to the spectra: hydrogen-poor Type I SLSNe (or SLSNe-I) and hydrogen-rich Type II SLSNe (or SLSNe-II). SLSNe-II can be explained as an interaction between the SN ejecta and dense circumstellar medium (CSM; e.g., Woosley et al. 2007), while a number of models have been proposed for SLSNe-I: a large amount of ^{56}Ni pro-

duced by a pair-instability SN (e.g., Woosley et al. 2007), spin-down of a newborn strongly magnetized neutron star (magnetar; e.g., Kasen & Bildsten 2010; Woosley 2010), fallback accretion onto a compact remnant (e.g., Dexter & Kasen 2013), and interaction with dense CSM (e.g., Smith & McCray 2007; Chevalier & Irwin 2011).

Radio observations can probe synchrotron emission arising from shock interaction of SN ejecta or jet with surrounding material, providing useful constraints on the models of SLSNe. It is expected that late-time radio emission may be caused by initially off-axis jets that decelerate and spread into the line of sight. It is also predicted that quasistate synchrotron emission may arise from pulsar wind nebulae (PWNe) powered by a newly born magnetar (Metzger & Bower 2014; Murase et al. 2016; Kashiyama & Murase 2017; Metzger et al. 2017). The radio emission is initially absorbed in the PWNe and SN ejecta, but the system can be transparent on timescales of decades. These central engine models are also a possible model for long-duration gamma-ray bursts (LGRBs) (e.g., Metzger et al. 2015; Margalit et al. 2018b), suggesting a connection between SLSNe-I and LGRBs. It is interesting that the magnetar model is also one of the plausible models for fast radio bursts (FRBs), which are mysterious radio transients with millisecond-scale bright flashes (Cordes & Chatterjee 2019, for a review). Magnetar models have been applied to the origin of FRB 121102 (e.g., Murase et al. 2016; Kashiyama & Murase 2017; Metzger et al. 2017; Margalit et al. 2018a; Margalit & Metzger 2018). Recently, FRB 200428 was identified as a Galactic magnetar, SGR 1935+2154 (Andersen et al. 2020; Bocherek et al. 2020), showing a magnetar origin of at least one FRB.

Previous radio observations of SLSNe resulted in non-detections in most cases, providing constraints on physical properties (such as energies, mass-loss rates, and CSM densities) and models for SLSNe-I (e.g., Nicholl et al. 2016, 2018; Margalit et al. 2018b; Bose et al. 2018; Coppejans et al. 2018; Law et al. 2019; Eftekhari et al. 2021). Eftekhari et al. (2019) found an unresolved radio source coincident with the position of SLSN-I PTF10hgi. They argued that the radio emission is consistent with an off-axis jet or wind nebula powered by a magnetar born in the SLSN, suggesting the presence of a central engine. Law et al. (2019) and Mondal et al. (2020) also supported the model of magnetar-powered SLSN based on the observations at 0.6–15 GHz. Hatsukade et al. (2021) found a variability in late-time radio emission in PTF10hgi for the first time among SLSNe. They constrained both the rise and decay phases of the radio light curve over three years, peaking at approximately 8–9 yr after the explosion. They concluded that plausi-

ble scenarios are a low-luminosity active galactic nucleus (AGN) in the host galaxy or a magnetar wind nebula by considering the radio light curve and spectrum.

In order to constrain the models, it is also important to understand the properties of their host galaxies. Previous studies have shown that SLSN-I hosts are typically dwarf galaxies with low-luminosity, low stellar mass, low star-formation rate (SFR), and high specific SFR (sSFR) compared to local star-forming galaxies and the hosts of core-collapse SNe, while SLSN-II hosts show a wider range of those parameters (e.g., Lunnan et al. 2014; Leloudas et al. 2015a; Angus et al. 2016; Perley et al. 2016; Chen et al. 2017; Schulze et al. 2018; Taggart & Perley 2021). The observations of SLSN hosts have been conducted mainly in the optical/near-infrared (NIR) wavelengths, which are subject to dust extinction in contrast to longer wavelengths, and it is possible that we are missing dust-obscured star formation. Radio observations are important to probe the properties of star formation in the SLSN host without the effect of dust extinction (Schulze et al. 2018; Hatsukade et al. 2018; Arabsalmani et al. 2019; Hatsukade et al. 2020; Eftekhari et al. 2021). Schulze et al. (2018) searched radio emission for a sample of SLSN hosts by using the survey data of Faint Images of the Radio Sky at Twenty-Centimeters (FIRST; Becker et al. 1995), the NRAO VLA Sky Survey (NVSS; Condon et al. 1998), and the Sydney University Molonglo Sky Survey (SUMSS; Bock et al. 1999), and did not find radio detection. They also obtained upper limits on three SLSN hosts based on deep 1.5 GHz observations with the Karl G. Jansky Very Large Array (VLA). Hatsukade et al. (2018) performed 3 GHz radio observations of the host galaxies of 8 SLSNe (5 Type I and 3 Type II) at $0.1 < z < 0.3$ with VLA. They found the excess of radio-based SFRs over extinction-corrected optically based SFRs (UV-based SFRs from SED fitting or H α -based SFRs) in three hosts, suggesting the existence of dust-obscured star formation that were missed in previous observations. This indicates the necessity of longer-wavelength observations in order to understand true star-forming activity in SLSN hosts. They also found that three hosts, which were located within the range of the main sequence based on previous optical observations, are actually above the main sequence in our radio observations, suggesting that they have a starburst nature. Eftekhari et al. (2021) observed 15 SLSNe-I at 6 GHz with VLA and 29 SLSNe-I at 100 GHz with the Atacama Large Millimeter/submillimeter Array (ALMA), seven of which overlapped. They did not detect emission from any of the SLSNe except for a 6 GHz detection of PTF10hgi. Only the host of PTF12dam was detected

at 6 GHz, concluding that there is no significant dust obscuration in the SLSNe hosts.

In this paper, we present the results of VLA 3 GHz continuum observations of 23 SLSNe (15 Type I and 8 Type II) and their host galaxies, offering one of the largest sample of SLSNe with radio data. The remainder of the paper is organized as follows. Section 2 describes targets, VLA observations, and data reduction. The results are shown in Section 3. In Section 4, we discuss a magnetar model for the SLSNe and obscured star formation in the host galaxies. Conclusions are presented in Section 5. Throughout the paper, we adopt a Chabrier (2003) initial mass function and cosmological parameters of $H_0 = 67.7 \text{ km s}^{-1} \text{ Mpc}^{-1}$ and $\Omega_M = 0.310$ based on the *Planck* 2018 results (Planck Collaboration et al. 2020).

2. VLA OBSERVATIONS

2.1. Targets

In order to understand the general properties of SLSNe and their hosts, it is essential to conduct an unbiased search for radio emission by using a complete sample. The targets of VLA observations were selected from the list of SLSNe compiled by Schulze et al. (2018). They made a list of 69 SLSNe discovered before the end of 2014 among all SLSNe reported in the literature, providing the largest and complete catalog of SLSNe. The redshifts of the sample are $z = 0.1\text{--}2$ with a singular object at $z = 3.899$, and the median redshifts are $z = 0.46$ and 0.21 for SLSNe-I and SLSNe-II, respectively. From the list, we selected SLSNe well observable with VLA (declination > -25 deg) and located at $z < 0.3$ to ensure significant constraint on obscured star formation. In order to avoid the contamination from AGN to radio emission, we excluded CSS100217, whose host is known to have possible AGN features (Leloudas et al. 2015a; Perley et al. 2016; Schulze et al. 2018). We also excluded six SLSNe (PTF10aagc, PTF11rks, SN2005ap, SN2008am, SN2008fz, and SN2010gx) that already have deep radio upper limits as reported in Hatsukade et al. (2018) and Schulze et al. (2018). This results in 23 targets that consists of 15 Type I and 8 Type II SLSNe (Table 1). This is one of the largest samples of SLSNe with radio observations. All of them were observed in the VLA 1.4 GHz surveys of FIRST and NVSS, and none was detected in relatively shallow observations (~ 0.15 and $\sim 0.45 \text{ mJy beam}^{-1}$, respectively; Schulze et al. 2018). In order to examine the time variability of the radio emission, four SLSNe (SN1999bd, PTF10qaf, PTF10uhf, PTF12dam) with radio detection

by Hatsukade et al. (2018) were included. Four SLSNe (SN1999bd, PTF10qaf, PTF10uhf, PTF12dam) whose hosts were detected in previous observations (Hatsukade et al. 2018) were included in the targets in order to examine the time variability of the radio emission. Our observations of these radio-detected sources were conducted $\gtrsim 2$ yr after the first observations, allowing us to examine the time variability. Detections of radio emission from PTF10hgi were reported by Eftekhari et al. (2019), Law et al. (2019), and Mondal et al. (2020) after the target selection of this work. Our VLA observations of PTF10hgi were reported in detail in a separate paper (Hatsukade et al. 2021).

We note previous radio observations of the targets at $\sim 1\text{--}10$ GHz. Existing radio observations of SLSNe and their hosts are compiled by Coppejans et al. (2018), Schulze et al. (2018), and Eftekhari et al. (2021). Of our targets, PTF09cnd, SN 2012il, and SN 2015bn were observed within a year after the explosions, yielding nondetections (Chandra et al. 2009, 2010; Chomiuk et al. 2012; Nicholl et al. 2016; Alexander et al. 2016). Late-time radio observations (\gtrsim a few years after the explosions) by Law et al. (2019) and Eftekhari et al. (2021) covered a fraction of the SLSNe-I in our sample; PTF09cnd, PTF10hgi, SN 2007bi, SN 2010kd, and SN 2011ke at 3 GHz by Law et al. (2019); LSQ12dlf, PTF09cnd, PTF12dam, SN 1999as, SN 2007bi, SN 2010kd, SN 2011ke, SN 2011kf, SN 2012il at 6 GHz by Eftekhari et al. (2021).

2.2. Observations and Data Reduction

The VLA S-band 3 GHz (13 cm) observations were performed from November 2018 to February 2019 in semester 18B (Project ID: 18B-077) and from April to June 2020 in semester 20A (Project ID: 20A-133). The observing dates are 5–21 yr after the discovery of the SLSNe. Observations were done in the array configuration C except for six targets (SN2007bw, SN2008es, SN2009nm, SN2010kd, SN2011ep, and SN2012il) that were observed during a transition period from configuration C to B. The number of antennae used in the observations was 24–28. The WIDAR correlator was used with 8-bit samplers. We used two basebands with 1 GHz bandwidth centered at 2.5 GHz and 3.5 GHz, which provided a total bandwidth of 2 GHz. The field of view was 7.4 (full width at half power). The positions of the SNe were used as phase centers. Bandpass and amplitude calibrations were conducted with 3C147 or 3C286, and phase calibrations were conducted with nearby quasars. The total observing time of each target

Table 1. Targets

SLSN	Discovery Date ^a	Type	z	$\log \text{SFR}^b$ ($M_{\odot} \text{ yr}^{-1}$)	$\log M_*^b$ (M_{\odot})
CSS121015 ^c	2012-10-15	II	0.286	$-0.52^{+0.38}_{-0.29}$	$8.15^{+0.15}_{-0.17}$
LSQ12dlf	2012-07-10	I	0.255	$-1.36^{+0.54}_{-0.43}$	$7.56^{+0.33}_{-0.34}$
LSQ14mo	2014-01-30	I	0.2561	$-0.84^{+0.42}_{-0.34}$	$7.89^{+0.15}_{-0.19}$
PTF09cnd	2009-08-07	I	0.258	$-0.64^{+0.21}_{-0.18}$	$7.87^{+0.20}_{-0.21}$
PTF10hgi ^d	2010-05-15	I	0.0987	$-1.02^{+0.44}_{-0.52}$	$7.58^{+0.29}_{-0.31}$
PTF10qaf	2010-08-05	IIIn	0.284	$0.11^{+0.50}_{-0.50}$	$8.73^{+0.22}_{-0.25}$
PTF10uhf	2010-08-25	I	0.2882	$0.834^{+0.122}_{-0.263}$	$11.23^{+0.15}_{-0.12}$
PTF12dam	2012-04-10	I	0.107	$-0.00^{+0.27}_{-0.26}$	$8.89^{+0.15}_{-0.30}$
SN 1999as	1999-02-18	I	0.127	$0.14^{+0.37}_{-0.35}$	$8.94^{+0.20}_{-0.17}$
SN 1999bd	1999-02-19	IIIn	0.151	$0.037^{+0.118}_{-0.162}$	$9.10^{+0.22}_{-0.11}$
SN 2006gy	2006-09-18	IIIn	0.019	$-1.12^{+0.08}_{-0.08}$	$11.70^{+0.06}_{-0.21}$
SN 2006tf ^e	2006-12-12	IIIn	0.074	$-1.25^{+0.48}_{-0.37}$	$7.54^{+0.47}_{-0.20}$
SN 2007bi ^f	2007-04-06	I	0.128	$-1.71^{+0.53}_{-0.52}$	$7.92^{+0.20}_{-0.21}$
SN 2007bw ^g	2007-04-18	IIIn	0.140	$-0.24^{+0.47}_{-0.37}$	$9.39^{+0.19}_{-0.09}$
SN 2008es ^h	2008-04-26	II	0.205	$-1.99^{+0.28}_{-0.27}$	$6.19^{+0.33}_{-0.36}$
SN 2009nm ⁱ	2009-11-20	IIIn	0.210	$-0.60^{+0.65}_{-0.62}$	$8.65^{+0.33}_{-0.34}$
SN 2010kd	2010-11-14	I	0.101	$-0.98^{+0.44}_{-0.31}$	$7.30^{+0.25}_{-0.29}$
SN 2011ep ^j	2011-04-14	I	0.280	$0.05^{+0.41}_{-0.30}$	$7.79^{+0.42}_{-0.36}$
SN 2011ke ^k	2011-04-06	I	0.143	$-0.82^{+0.24}_{-0.23}$	$7.50^{+0.20}_{-0.18}$
SN 2011kf ^l	2011-12-30	I	0.245	$-0.86^{+0.18}_{-0.20}$	$7.58^{+0.19}_{-0.22}$
SN 2012il ^m	2012-01-19	I	0.175	$-0.74^{+0.22}_{-0.36}$	$8.20^{+0.18}_{-0.17}$
SN 2013dg ⁿ	2013-05-17	I	0.265	$-1.43^{+0.80}_{-0.52}$	$7.09^{+0.82}_{-0.70}$
SN 2015bn ^o	2014-12-23	I	0.110	$-1.06^{+0.69}_{-0.50}$	$7.50^{+0.38}_{-0.35}$

^aDiscovery date (maximum date for PTF10qaf) taken from Open Supernova Catalog^a (Guillochon et al. 2017).

^bSFR and stellar mass of host galaxies derived from SED modeling by Schulze et al. (2018).

^cAlias: CSS121015:004244+132827

^dAliases: SN 2010md, PSO J249.4461+06.2081.

^eAlias: CSS070320:124616+112555.

^fAlias: SNF20070406-008.

^gAlias: SNF20070418-020.

^hAlias: ROTSE3 J115649.1+542726.

ⁱAlias: CSS091120:100525+511639.

^jAlias: CSS110414:170342+324553.

^kAliases: CSS110406:135058+261642, PS1-11xk, PTF11dij.

^lAlias: CSS111230:143658+163057.

^mAliases: CSS120121:094613+195028, PS1-12fo.

ⁿAliases: CSS130530:131841-070443, MLS130517:131841-070443.

^oAliases: CSS141223:113342+004332, MLS150211:113342+004333, PS15ae.

^a <https://sne.space/>

Table 2. VLA 3 GHz Observations

SLSN	Obs. Date	Time Since Expl. ^a	T_{on}	N_{ant}	Baseline	Beam Size	P.A.	RMS	$S_{3\text{GHz}}$
		(yr)	(min)		(m)	($''$)	($^{\circ}$)	($\mu\text{Jy beam}^{-1}$)	(μJy)
(1)	(2)	(3)	(4)	(5)	(6)	(7)	(8)	(9)	(10)
CSS121015	2019-01-02	4.8	91	27	45–3400	8.4×5.4	−1.6	5.7	< 17
LSQ12dlf	2019-01-03	5.2	91	26	45–3400	13.0×5.2	4.7	6.4	< 19
...	2020-04-01	6.2	103	27	45–3400	11.7×5.7	12.6	6.1	< 18
...	combined	12.1×5.5	8.4	5.3	< 16
LSQ14mo	2020-04-19	4.9	103	27	45–3400	10.4×5.7	−11.2	7.0	< 21
PTF09cnd	2018-11-27	7.4	91	24	78–3400	8.2×4.9	−15.8	5.4	< 16
PTF10hgi	2018-12-02	7.8	91	26	45–3400	8.9×5.8	42.7	5.3	85 ± 7^b
...	2020-04-25	9.1	103	28	45–3400	7.8×6.3	43.5	5.8	51 ± 6^b
PTF10qaf	2017-05-29	1.9	91	27	45–3400	8.1×6.1	−49.1	5.4	58 ± 6^c
...	2020-04-06	4.1	103	27	45–3400	8.1×6.1	49.6	6.9	57 ± 8^c
...	combined	6.9×6.7	86.4	4.9	57 ± 6^c
PTF10uhf	2017-05-29	5.2	91	27	45–3400	6.7×5.5	73.5	5.4	82 ± 7^d
...	2020-06-08	7.6	103	27	45–3400	7.7×5.7	89.7	5.4	77 ± 7^d
...	combined	7.0×5.6	82.8	4.0	77 ± 6^d
PTF12dam	2017-05-28	4.6	91	27	45–3400	6.5×5.6	68.8	4.5	139 ± 8^e
...	2020-06-06	7.4	103	26	45–3200	7.0×5.4	67.2	4.6	131 ± 8^e
...	combined	6.5×5.6	82.8	3.5	133 ± 8^e
SN 1999as	2019-01-14	17.7	91	24	45–3400	6.9×5.8	−50.3	5.5	< 17
SN 1999bd	2017-05-28	15.9	91	27	45–3400	6.2×5.3	−2.8	5.2	43 ± 6^f
...	2020-04-14	18.4	103	26	45–3400	6.2×5.6	22.4	5.4	37 ± 6^f
...	combined	6.0×5.4	−11.7	4.0	41 ± 5^f
SN 2006gy	2019-01-01	12.1	91	25	45–3400	6.2×5.3	−63.0	44	838 ± 61^g
...	2020-03-16	13.2	103	27	45–3400	5.8×5.2	74.7	43	859 ± 61^g
...	combined	6.0×5.3	−69.8	38	859 ± 57^g
SN 2006tf	2020-06-04	12.5	103	26	45–3400	6.7×5.8	−0.8	5.0	< 15
SN 2007bi	2020-05-22	11.6	103	27	45–3400	8.8×5.9	52.5	7.1	< 21
SN 2007bw	2019-02-19	10.4	91	27	45–11100	3.2×2.2	14.9	4.6	< 14
SN 2008es	2019-02-17	9.0	91	27	45–11100	3.6×1.9	49.2	4.2	< 12
SN 2009nm	2019-02-19	7.6	91	27	45–11100	3.4×1.8	21.6	4.1	< 12
SN 2010kd	2019-02-19	7.5	91	27	45–11100	3.3×1.8	21.4	3.9	< 12
SN 2011ep	2019-02-22	6.1	91	26	80–11100	3.4×2.2	42.2	4.3	< 13
SN 2011ke	2020-04-24	7.9	109	28	45–3400	6.7×6.4	69.6	4.3	< 13
SN 2011kf	2020-06-05	6.8	103	27	45–3400	9.8×5.8	−58.4	6.1	< 18
SN 2012il	2019-02-22	6.0	91	26	80–11100	3.4×1.7	2.3	4.0	< 12
SN 2013dg	2020-06-06	5.6	103	27	45–3400	8.9×6.0	−8.3	24	< 72
SN 2015bn	2020-06-07	4.9	103	27	45–3400	11.2×6.5	51.9	15	< 45

NOTE— (1) SLSN name. (2) VLA observing date. “combined” is for the combined results of two observations. (3) Time since explosion (rest frame). (4) On-source integration time. (5) Number of antennas. (6) Range of baseline lengths. (7) Synthesized beam size. (8) Position angle of synthesized beam. (9) RMS noise level of the map. (10) Flux density at 3 GHz. Limits are 3σ .

^aExplosion rest frame.

^bLikely to be from both SN and host; [Hatsukade et al. \(2021\)](#)

^cLikely to be from host.

^dIntegrated intensity measured with the CASA `imfit` task. Likely to be from host.

^eLikely to be from host (SDSS J142446.21+461348.6).

^fLikely to be from host (A093029+1626).

^gLikely to be from host (NGC 1260).

was 91–109 min. Details of the observations appear in Table 2.

The data were reduced with Common Astronomy Software Applications (CASA; McMullin et al. 2007) release 5.6.2. About 10%–15% of the data were flagged by the pipeline processing. The maps were produced with the task `tclean`. The Briggs weighting with `robust` 0.5 was adopted. The absolute flux accuracy was estimated by comparing the measured flux density of the amplitude calibrators and the flux density scale of Perley & Butler (2017), and the difference was found to be <2%. For detected sources, we conducted a 2D Gaussian fit to the radio emission in the image plane. PTF10uhf was spatially resolved, and we measured an integrated flux density by using the `imfit` task. The others were not spatially resolved or only marginally resolved and we adopted the peak intensity as a source flux density. The flux uncertainty reported here is a combination of the map rms and a 5% absolute flux calibration uncertainty¹.

We also reanalyzed the VLA data of Hatsukade et al. (2018) of four SLSNe (PTF10qaf, PTF10uhf, PTF12dam, and SN 1999bd) that were included in the sample of this study by using the same version of CASA as used in this work. Although Hatsukade et al. (2018) reported that PTF10qaf is spatially resolved, we found that the emission is only marginally resolved, and we adopted a peak intensity as a source flux density in this work. In order to create deeper images, we combined the data of Hatsukade et al. (2018) with the newly obtained data except for PTF10hgi, which showed a time variability. The results are included in Table 2.

3. RESULTS

The VLA 3 GHz continuum maps are shown in Figure 1. We detected radio emission in six sources (PTF10hgi, PTF10qaf, PTF10uhf, PTF12dam, SN 1999bd, SN 2006gy) with a peak signal-to-noise ratio (S/N) above 5, and tentatively detected in two sources (SN 2007bw and SN 2012il) with S/N \sim 3.6. Five of them (PTF10hgi, PTF10qaf, PTF10uhf, PTF12dam, and SN 1999bd) were detected in the previous 3 and 6 GHz observations (Hatsukade et al. 2018; Law et al. 2019; Eftekhari et al. 2021), and the peak positions are consistent. SN 2006gy and PTF10hgi were detected in both semesters (18B and 20A) in our observations. Because the radio emission detected in the map of LSQ12dlf was \sim 3'' away from the SN position, which is larger than the positional uncertainty of the radio ob-

servations (\sim 2''), we consider that the emission is not associated with the SN or its host galaxy (Table 3). Figure 2 shows the radio contours for the six radio-detected sources overlaid on the optical/NIR images taken from the Hubble Legacy Archive² and the public data of the Dark Energy Survey (DES; Abbott et al. 2018; Morganson et al. 2018; Flaughner et al. 2015). The radio emission of PTF10qaf, PTF10uhf, and SN 2006gy are dominated by the galaxy center rather than the SN positions. The radio peak position of PTF12dam is also slightly offset from the SN position and close to the galaxy center. This is supported by the higher angular resolution ($0''.95 \times 0''.74$) observations at 6 GHz by Eftekhari et al. (2021), who claimed that the emission was most likely related to star formation in the host. The peak radio position of SN 1999bd appears to be associated with a faint object \sim 2'' south of the SN position. While the apparent distance between the radio peak and the SN position is still within the uncertainty of the radio observations, it is not clear whether the emission comes from the SN or its host galaxy. It is possible that the radio emission arose from an unassociated foreground/background galaxy.

To see whether the sources show a time variability, we plot the observed flux densities as a function of time in Figure 3 including previous 3 GHz observations by Eftekhari et al. (2019) and Mondal et al. (2020) for PTF10hgi. A significant variability is found in PTF10hgi, which was reported by Hatsukade et al. (2021). The flux densities of SN 1999bd appear to be decreasing with time but are still consistent within flux uncertainties. The other sources do not show a significant variability in the timescale of years, suggesting the emission arise from activity in the hosts. This is supported by the fact that the emission of PTF10qaf, PTF10uhf, and SN 2006gy are dominated by the galaxy center rather than the SN positions.

In the following discussions, we adopt the 3 GHz flux densities for the six $>5\sigma$ sources and 3σ upper limits for the remaining sources. We consider that the origin of the radio emission is likely to be activities in the hosts for PTF10qaf, PTF10uhf, PTF12dam, SN 1999bd, and SN 2006gy, and the SN and/or the host for PTF10hgi (Hatsukade et al. 2021).

4. DISCUSSION

Late-time radio observations provide useful implications for the obscured star formation in the host galaxies and power source of SLSNe. By using the radio data,

¹ <https://science.nrao.edu/facilities/vla/docs/manuals/oss/performance/fdscale>

² <https://hla.stsci.edu/>

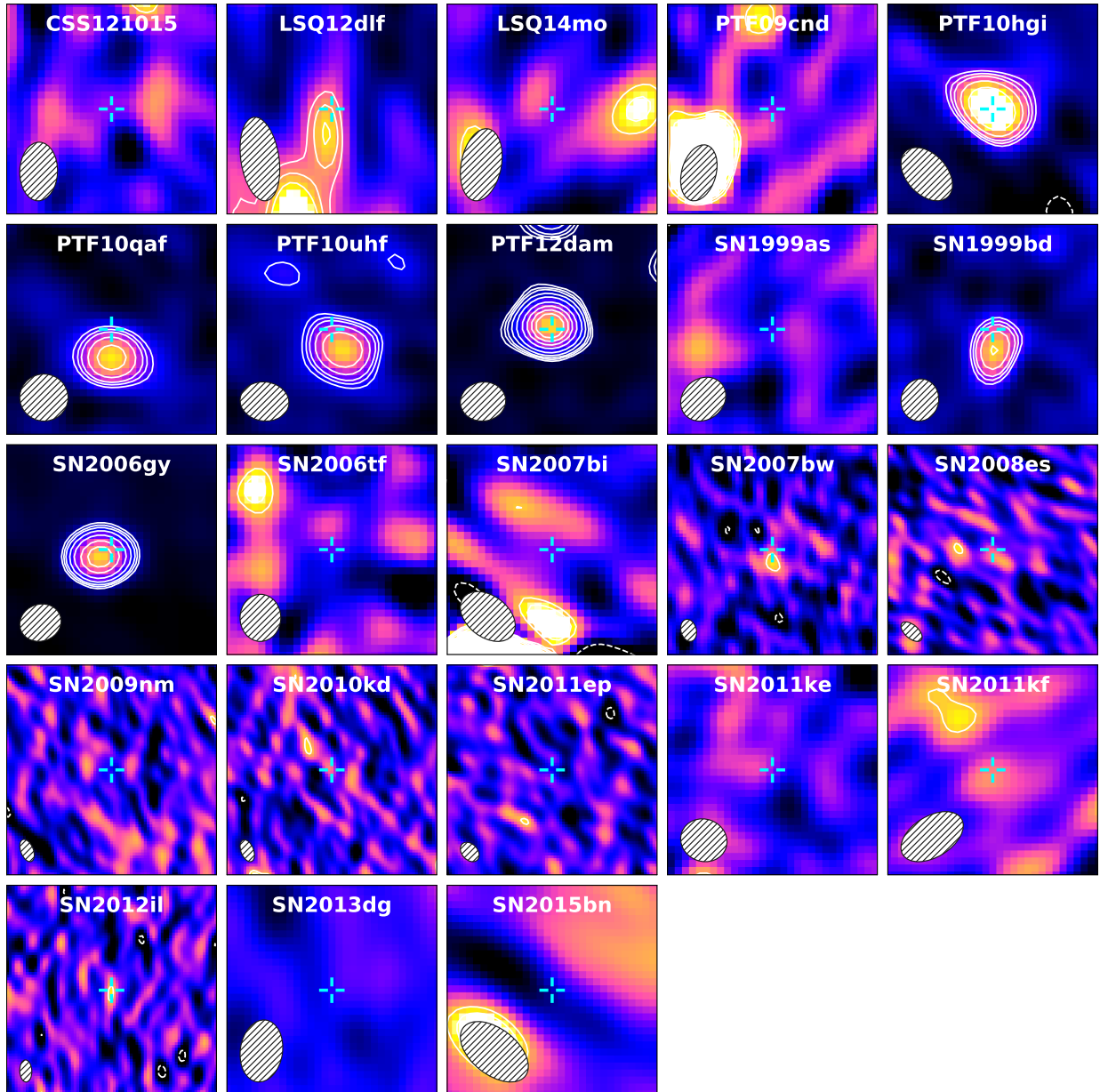


Figure 1. VLA 3 GHz continuum maps centered at SN positions. Image size is $30'' \times 30''$. North is up, and east is to left. Crosses represent SN positions. Contours are -3σ , 3σ , 4σ , 5σ , 7σ , 10σ , and 5σ steps subsequently (negative contours as dashed). Synthesized beam size is shown at lower left corners. Image of SN 2006gy is based on combined data of two observations in this study, and images of PTF10qaf, PTF10uhf, PTF12dam, and SN 1999bd are based on combined data of this study and Hatsukade et al. (2018). Image of PTF10hgi is based on data taken in 2018.

we constrain radio emission arising from star-forming activities in the hosts (Section 4.1), off-axis afterglows (Section 4.2), and pulsar/magnetar wind nebulae (Section 4.3).

4.1. Obscured Star Formation in Host Galaxies

In the Baldwin-Phillips-Terlevich (BPT; Baldwin et al. 1981) diagram, the hosts of PTF09cnd, PTF10qaf, PTF12dam, and SN 1999bd lie at the location of star-

forming galaxies (Leloudas et al. 2015a; Perley et al. 2016). Because the radio emission in PTF10hgi may arise from an AGN in the host or wind nebula powered by a magnetar (Hatsukade et al. 2021), the flux density is treated as an upper limit for star-forming activity in the host. Assuming that the radio emission of detected hosts is dominated by star-forming activity, we derive SFRs by using the 3 GHz flux densities. SFRs are derived by adopting the calibrations of Murphy et al. (2011,

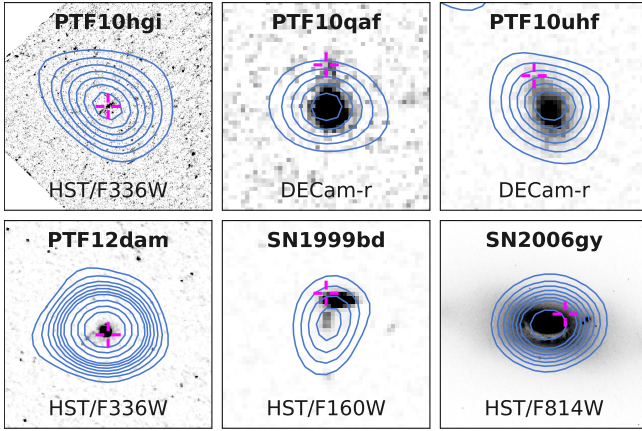


Figure 2. VLA 3 GHz contours overlaid on optical/NIR images for radio-detected ($>5\sigma$) sources centered at radio peak positions. Image size is $20'' \times 20''$. North is up, and east is to left. Crosses represent SN positions. Contour levels are same as in Figure 1.

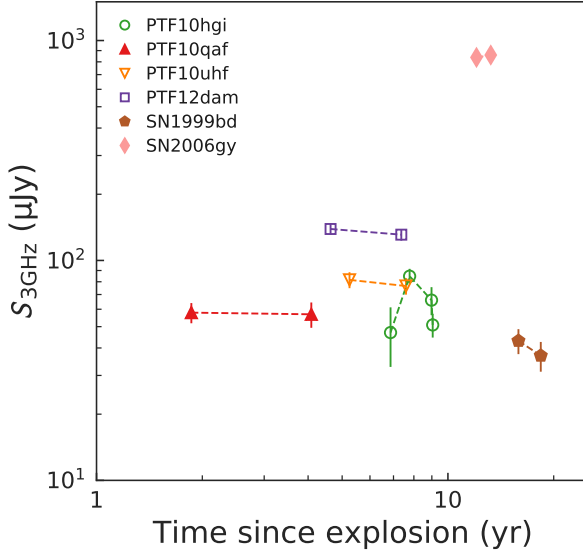


Figure 3. Observed 3 GHz flux densities as function of time since explosion (rest frame) for radio-detected sources. Open and filled symbols represent SLSNe-I and SLSNe-II, respectively. Data points of PTF10hgi include results of Law et al. (2019), Mondal et al. (2020), and Hatsukade et al. (2021).

2012, 2017) normalized to the Chabrier (2003) IMF as follows (Jiménez-Andrade et al. 2021):

$$\text{SFR} = 4.87 \times 10^{-29} L_{1.4 \text{ GHz}}, \quad (1)$$

$$L_{1.4 \text{ GHz}} = \frac{4\pi D_L^2}{(1+z)^{1+\alpha}} \left(\frac{1.4}{\nu_{\text{obs}}} \right)^\alpha S_{\text{obs}}, \quad (2)$$

where $L_{1.4 \text{ GHz}}$ is the 1.4 GHz luminosity in $\text{erg s}^{-1} \text{ Hz}^{-1}$, D_L is the luminosity distance in cm, α

Table 3. Offset between radio peak and SN positions.

SLSN	Offset (arcsec)
PTF10hgi	0.7
PTF10qaf	4.0
PTF10uhf	3.6
PTF12dam	0.0
SN 1999bd	3.0
SN 2006gy	2.3

is the spectral index (defined as $S_\nu \propto \nu^\alpha$), ν_{obs} is the observed frequency in GHz, and S_{obs} is the observed flux density in $\text{erg s}^{-1} \text{ cm}^{-2} \text{ Hz}^{-1}$. If a source was observed twice, then the flux density of combined analysis (Table 2) is used. The spectral index α is known to lie between around -0.8 and -0.7 for star-forming galaxies (e.g., Condon 1992). Smolčić et al. (2017a) and Delhaize et al. (2017) found that the median spectral index between 1.4 and 3 GHz for $z < 2$ star-forming galaxies is consistent with $\alpha_{1.4\text{GHz}}^{3\text{GHz}} = -0.7$ with a standard deviation of $\sigma = 0.35$ based on the VLA-COSMOS 3 GHz data taking into account the lower limits for sources undetected at 1.4 GHz. In this study we assume $\alpha = -0.7$ following these studies. The derived 1.4 GHz luminosities and SFRs are listed in Table 4. Note that the SFRs would increase by about 10% if we assume $\alpha = -0.8$.

We employed a stacking analysis on the 3 GHz maps of the undetected sources to obtain “averaged” properties of the hosts. No significant emission was detected for the samples of all 15 nondetections, 11 SLSNe-I, and 4 SLSNe-II. The obtained rms noise levels were 1.4, 1.8, and $2.3 \mu\text{Jy beam}^{-1}$ for the samples of all nondetections, SLSNe-I, and SLSNe-II, respectively. In order to constrain obscured star formation, we derived SFRs from stacking analysis. Because the sample of nondetections covers a wide redshift range ($z = 0.074\text{--}0.287$), where luminosity distances largely differ among the samples, we divided the sample into two groups: 6 SLSNe with $z = 0.074\text{--}0.143$ ($z_{\text{median}} = 0.12$) and 9 SLSNe with $z = 0.205\text{--}0.287$ ($z_{\text{median}} = 0.26$). The stacked images show no significant emission with rms noise levels of 2.2 and $1.8 \mu\text{Jy beam}^{-1}$, respectively. The corresponding 3σ upper limits on SFRs are <0.20 and $<0.88 M_\odot \text{ yr}^{-1}$, respectively, which were calculated in the same manner as for individual hosts assuming the median redshifts (Table 5).

In Figure 4, we compare the SFRs derived from the radio observations with those from the SED modeling based on multi-wavelength data from rest-frame UV to NIR by Schulze et al. (2018). Because of the complexity of star-formation histories of the hosts of SN 1999bd and SN 2006gy, Schulze et al. (2018) adopted the H α of Leloudas et al. (2015b) and the IR luminosity of Smith et al. (2007) as an SFR indicator instead of using the results of SED analysis. The hosts of PTF10qaf, PTF10uhf, PTF12dam, and SN 1999bd have an excess of radio-based SFRs over SED-based SFRs by a factor of 3–12. The radio excess in the hosts of SN 1999bd, PTF10qaf, and PTF10uhf are consistent with the results by (Hatsukade et al. 2018). On the other hand, Hatsukade et al. (2018) and Eftekhari et al. (2021) did not find a radio excess in the PTF12dam host. This is due to the difference in comparison SFRs adopted by Hatsukade et al. (2018) and Eftekhari et al. (2021), where they used the results of Perley et al. (2016). The H α -based SFR of 3–5 M_{\odot} yr $^{-1}$ (Leloudas et al. 2015a; Thöne et al. 2015; Chen et al. 2015; Perley et al. 2016) is consistent with our radio SFR of $3.4 \pm 0.2 M_{\odot}$ yr $^{-1}$. The same is true of PTF10uhf, where the radio SFR of $17 \pm 1 M_{\odot}$ yr $^{-1}$ is consistent with the extinction-corrected H α SFR of $19.36^{+7.301}_{-5.764} M_{\odot}$ yr $^{-1}$ (Perley et al. 2016). Schulze et al. (2018) noted that a systematic uncertainty of 0.3 dex is expected in the SED-based SFRs. Therefore, the existence of obscured star formation in the hosts of PTF10uhf and PTF12dam is inconclusive. Optical observations show that a dwarf galaxy hosting PTF10qaf is likely to be interacting with a large spiral galaxy (Perley et al. 2016). The optical image of the PTF10uhf host is also likely to represent a merger (Perley et al. 2016). The interaction or merger may cause dusty star formation in the hosts. The stellar masses of the hosts of SN 1999bd, SN 2006gy, PTF10qaf, and PTF10uhf are in the largest range among the sample of SLSNe (Leloudas et al. 2015a; Perley et al. 2016; Schulze et al. 2018). In particular, the hosts of SN 2006gy and PTF10uhf have the largest stellar mass with $\log M_{*}/M_{\odot} > 11$ (Perley et al. 2016; Schulze et al. 2018). It is known that larger stellar mass galaxies have higher fraction of obscured star formation (e.g., Whitaker et al. 2017). Whitaker et al. (2017) found that more than 90% of star formation is obscured for galaxies with $\log M_{*}/M_{\odot} > 10.5$. Although the host of SN 2006gy, NGC 1260, is a S0/Sa galaxy, it shows signatures of current star formation with a far-IR luminosity of $\log L_{\text{FIR}}/L_{\odot} = 9.85$ (Meusinger et al. 2000; Smith et al. 2007). The IR-based SFR is $0.9 M_{\odot}$ yr $^{-1}$, which is comparable to the radio-based SFR.

For the other SLSN hosts, we do not find a significant excess of the radio-based SFRs over the SED-based SFRs, although many of them have upper limits. The fact that there is no significant dust-obscured star formation in SLSN hosts is consistent with the radio observations by Schulze et al. (2018) and Eftekhari et al. (2021) for individual galaxies or stacked results.

In Figure 5, we plot radio-based SFRs as a function of stellar mass. It is known that star-forming galaxies follow a tight correlation between stellar mass and SFR, referred to as a galaxy main sequence. The hosts of PTF10qaf and PTF12dam are located above the main sequence, suggesting that they have a starburst nature (e.g., Rodighiero et al. 2011; Elbaz et al. 2011). We note that if we adopt the stellar mass of $\log M_{*}/M_{\odot} = 10.24^{+0.22}_{-0.17}$ for PTF10qaf derived from the SED analysis by Leloudas et al. (2015a), the host is on the main sequence. The high sSFR and starburst nature of the PTF12dam host are consistent with the results of optical spectroscopic observations (Thöne et al. 2015; Chen et al. 2015). The SN 2006gy host is below the main sequence, suggesting a quenched property. This is consistent with its classification of S0/Sa, but at the same time the host has ongoing star formation as found in this work and previous studies (Smith et al. 2007). The other radio-detected hosts of SN 1999bd and PTF10uhf are within the range of the main sequence. The hosts of SLSNe are argued to have higher sSFR than main-sequence galaxies (e.g., Leloudas et al. 2015a; Schulze et al. 2018). Our results are consistent with these previous studies overall but are not stringent because of the limited sensitivity of the radio observations.

4.2. Afterglows from Off-axis Jet

A shock interaction between SN ejecta and CSM produces synchrotron radio emission. It is possible that radio afterglows arise from initially off-axis jets that decelerated and spread into the line of sight at late times. Coppejans et al. (2018) compiled all radio observations of SLSNe-I (9 SLSNe-I at that time) and constrained energies and mass-loss rates or CSM densities for an off-axis jet model. Eftekhari et al. (2021) generated a grid of afterglow models for a range of jet energies and CSM densities for the sample of 15 SLSNe-I and compared them with the upper limits at 6 and 100 GHz. They ruled out the presence of jets with an isotropic-equivalent energy $E_{\text{iso}} \gtrsim 10^{54}$ erg and CSM densities $n \sim 10^{-3}$ – 10^2 cm $^{-3}$ for observing angles $\theta_{\text{obs}} = 30$ and 60° .

Table 4. 1.4 GHz luminosities and radio-based SFRs of the hosts

SLSN	z	$L_{1.4\text{GHz}}^a$ ($\text{erg s}^{-1} \text{Hz}^{-1}$)	SFR ($M_{\odot} \text{yr}^{-1}$)
CSS121015	0.286	$< 7.4 \times 10^{28}$	< 3.6
LSQ12dlf	0.255	$< 5.4 \times 10^{28}$	< 2.6
LSQ14mo	0.2561	$< 7.2 \times 10^{28}$	< 3.5
PTF09cnd	0.258	$< 5.6 \times 10^{28}$	< 2.5
PTF10hgi	0.0987	$< 2.2 \times 10^{28}$	< 1.1
PTF10qaf	0.284	$(2.4 \pm 0.2) \times 10^{29}$	12 ± 1
PTF10uhf	0.2882	$(3.4 \pm 0.2) \times 10^{29}$	17 ± 1
PTF12dam	0.107	$(6.9 \pm 0.4) \times 10^{28}$	3.4 ± 0.2
SN 1999as	0.127	$< 1.2 \times 10^{28}$	< 0.6
SN 1999bd	0.151	$(4.5 \pm 0.5) \times 10^{28}$	2.2 ± 0.2
SN 2006gy	0.019	$(1.3 \pm 0.1) \times 10^{28}$	0.62 ± 0.04
SN 2006tf	0.074	$< 3.6 \times 10^{27}$	< 0.17
SN 2007bi	0.128	$< 1.6 \times 10^{28}$	< 0.79
SN 2007bw	0.140	$< 1.3 \times 10^{28}$	< 0.62
SN 2008es	0.205	$< 2.6 \times 10^{28}$	< 1.3
SN 2009nm	0.210	$< 2.7 \times 10^{28}$	< 1.3
SN 2010kd	0.101	$< 5.4 \times 10^{27}$	< 0.26
SN 2011ep	0.280	$< 5.4 \times 10^{28}$	< 2.6
SN 2011ke	0.143	$< 1.2 \times 10^{28}$	< 0.60
SN 2011kf	0.245	$< 5.7 \times 10^{28}$	< 2.8
SN 2012il	0.175	$< 1.8 \times 10^{28}$	< 0.87
SN 2013dg	0.265	$< 2.7 \times 10^{29}$	< 13
SN 2015bn	0.110	$< 2.5 \times 10^{28}$	< 1.3

NOTE— Errors only take into account flux measurement uncertainty (1σ). Limits are 3σ (except for PTF10hgi, where radio emission observed in April 2020 was used as an upper limit).

^aAssuming a spectral index of $\alpha_{1.4\text{GHz}}^{3\text{GHz}} = -0.7$.

Table 5. Results for stacking analysis of radio-undetected SLSN hosts

Sample	Number	z_{med}	RMS ($\mu\text{Jy beam}^{-1}$)	SFR ^a ($M_{\odot} \text{yr}^{-1}$)
$z < 0.2$	6	0.12	2.2	< 0.20
$z > 0.2$	9	0.26	1.8	< 0.88

^a 3σ upper limits on SFRs assuming spectral index of $\alpha_{1.4\text{GHz}}^{3\text{GHz}} = -0.7$ and median redshift z_{med} .

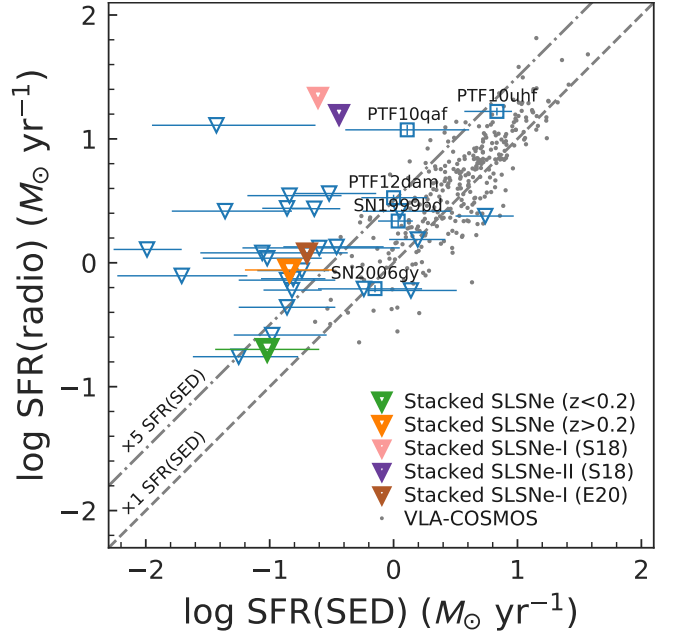


Figure 4. Comparison of SFRs derived from radio observations and SED analysis. Results on individual host and stacked results for radio-undetected SLSNe hosts are presented. SED-based SFRs are taken from Schulze et al. (2018) except for SN 1999bd and SN 2006gy, where H α -based SFR of Leloudas et al. (2015b) and IR-based SFR of Smith et al. (2007) are adopted. Triangles represent 3σ upper limits for nondetections. Stacked results on sample of nondetections (6 SLSNe at $z < 0.2$ as a green triangle and 9 SLSNe at $z > 0.2$ as an orange triangle) are plotted, where horizontal value and range are median and standard deviation of SFRs for sample (Schulze et al. 2018), respectively. We also plot stacked results by Schulze et al. (2018) (17 SLSNe-I and 13 SLSNe-II at $z < 0.5$) and Eftekhari et al. (2021) (13 SLSNe-I at $z < 0.4$). For comparison, star-forming galaxies without AGN feature from VLA-COSMOS survey source catalog (Smolčić et al. 2017a,b) at $z < 0.3$ (dots). Dashed and dot-dashed lines represent SFR(radio) equals to and five times SFR(SED), respectively.

By using our 3 GHz radio upper limits, we constrain the parameters for an afterglow model. We utilize the publicly available `afterglowpy` code (Ryan et al. 2020), which generates afterglow light curves using semi-analytic approximations of the jet evolution and synchrotron emission. The `afterglowpy` code has been calibrated to the `BoxFit` code (van Eerten et al. 2012) and produces similar light curves for on- and off-axis top hat jets. We adopted a top hat jet with following fixed parameters: jet opening angle of 10° , electron energy distribution index of $p = 2.5$, thermal energy fraction in electrons of $\epsilon_e = 0.1$, and thermal energy fraction in magnetic field of $\epsilon_B = 0.01$, which are typical values for GRBs (e.g., Wang et al. 2015); these values were

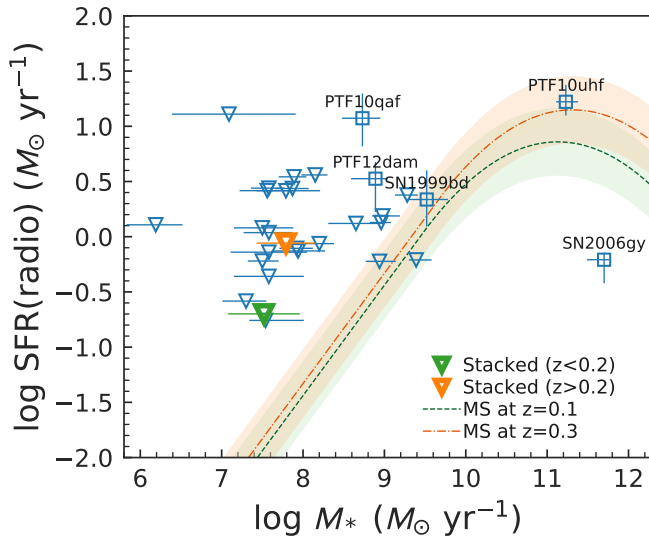


Figure 5. Radio-based SFRs as a function of stellar mass. Results on individual host and stacked results for radio-undetected hosts are presented. Horizontal value and range for stacked results are median and standard deviation for sample, respectively. Triangles represent 3σ upper limits. Dashed and dot-dashed curves show main-sequence of star-forming galaxies at $z = 0.1$ and 0.3 , respectively, with ± 0.3 dex uncertainty (Schreiber et al. 2015).

also assumed in previous studies (Eftekhari et al. 2019, 2021). We generated light curves with isotropic equivalent energies ranging from 10^{53} to 10^{55} erg, CSM densities ranging from 10^{-3} to 10^2 cm^{-3} , and viewing angles of 30 , 60 , and 90° . Figure 6 compares the VLA 3 GHz data with the model light curves with $E_{\text{iso}} = 10^{54}$ erg and $n = 10, 1, 0.1$, and 0.01 cm^{-3} . Figure 7 shows allowed parameters in $n - E_{\text{iso}}$ plots estimated for individual SLSN. We found that the radio upper limits exclude the models with i) $E_{\text{iso}} \gtrsim \text{several} \times 10^{53}$ erg and $n \gtrsim 10^{-3}$ cm^{-3} for $\theta_{\text{obs}} \sim 30$ – 60° and ii) $E_{\text{iso}} \gtrsim \text{several} \times 10^{53}$ erg and $n \gtrsim 10^{-2}$ cm^{-3} for $\theta_{\text{obs}} \sim 90^\circ$. Afterglows with lower energies or lower CSM densities are not excluded with the current data. The results are consistent with previous studies overall (Nicholl et al. 2016; Coppejans et al. 2018; Eftekhari et al. 2021). Further observations are required to constrain the afterglow models or parameters.

4.3. Pulsar/Magnetar Wind Nebulae

It is predicted that late-time radio emission may arise from PWNe caused by pulsar/magnetar-driven SLSNe-I (e.g., Metzger & Bower 2014; Murase et al. 2016; Kashiyama & Murase 2017; Metzger et al. 2017). Based on the model of Murase et al. (2015) and Murase et al. (2016), Omand et al. (2018) and Law et al. (2019) calculated radio light curves for samples of SLSNe-I with

maximum absorption and with no absorption processes in the PWN and SN ejecta. The initial parameters of a magnetar (spin period P_i , magnetic field B , and ejecta mass M_{ej}) were obtained by fitting the early optical light curves by eye. They defined two parameter sets for reproducing the optical light curves with $P = 1$ ms (P_{min}) and with the largest spin period (P_{max}). The radio emission can be absorbed in the PWN and the SN ejecta, but the system can be transparent in the timescale of years and reaches its peak at ~ 10 – 30 yr after the explosions. Eftekhari et al. (2021) considered two scenarios for PWNe: an ion-electron wind based on the prescription for FRB 121102 from Margalit & Metzger (2018), and an electron-positron wind following the methods of Murase et al. (2016), Omand et al. (2018), and Murase et al. (2021). The inferred magnetar parameters (ejecta mass and velocity, magnetar magnetic field and spin period) are derived via Markov chain Monte Carlo fits to the multi-color light curves using MOSFiT.

Our sample of SLSNe-I (except for PTF10uhf, SN1999as, and SN2011ep) are covered by these studies (Omand et al. 2018; Law et al. 2019; Eftekhari et al. 2021), and we compare our VLA results with their predictions based on electron-positron wind models. The 3 GHz upper limits on SN2011ke and SN2012il exclude the predictions by Omand et al. (2018) and Law et al. (2019) with or without absorption processes. The predictions without absorption for PTF09cnd by Law et al. (2019) and Eftekhari et al. (2021) and for SN2010kd by Law et al. (2019) are also excluded. While the predictions for SN2007bi by Eftekhari et al. (2021) both with or without absorption are excluded, the P_{min} model with absorption by Law et al. (2019) is still viable. The predictions for the remaining SLSNe-I cannot be ruled out in the current data. The outcomes are summarized in Table 6.

Finally, we constrain the pulsar/magnetar-driven model for SN2015bn by Murase et al. (2021). They found that the ALMA observations disfavors a PWN model motivated by the Crab nebula and argued that this tension can be resolved if the nebular magnetization is very high or very low. We found that at least the low-magnetization model without ejecta absorption is ruled out by our VLA 3 GHz upper limit.

5. CONCLUSIONS

We reported the results of VLA 3 GHz continuum observations of 23 SLSNe and their host galaxies 5–21 yr after the explosions. The sample consisted of 15 SLSNe-I and 8 SLSNe-II at $z < 0.3$. This study provided one of the largest samples of SLSNe with late-

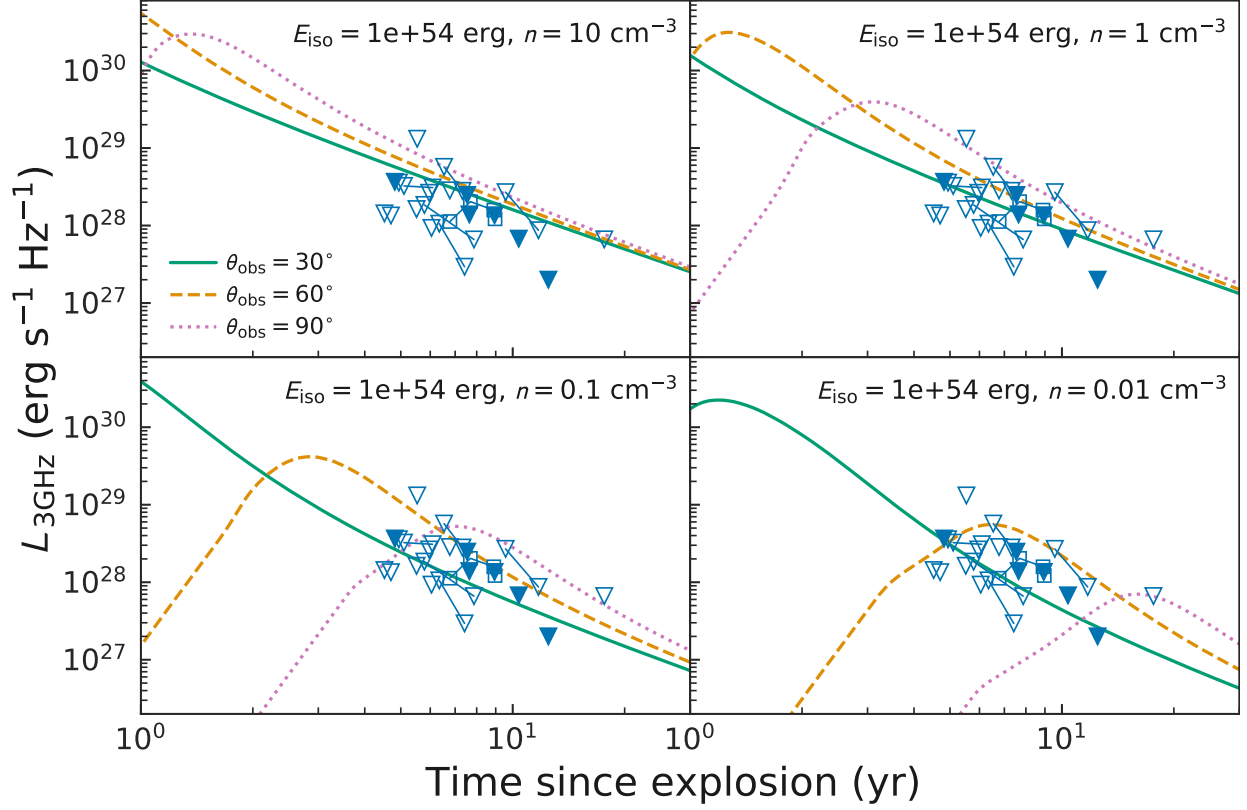


Figure 6. 3 GHz luminosities of SLSNe as a function of time since explosion (rest frame) in comparison with afterglow models generated using the `afterglowpy` code (Ryan et al. 2020) assuming a median redshift of the sample of $z = 0.19$ with $E_{\text{iso}} = 10^{54}$ erg and $n = 10 \text{ cm}^{-3}$ (top left), $n = 1 \text{ cm}^{-3}$ (top right), $n = 0.1 \text{ cm}^{-3}$ (bottom left), and $n = 0.01 \text{ cm}^{-3}$ (bottom right). Solid, dashed, and dotted curves represent light curves with viewing angles of $\theta_{\text{obs}} = 30^\circ$, 60° , and 90° , respectively. Triangles represent 3σ upper limits. Open and filled symbols represent SLSNe-I and SLSNe-II, respectively. SLSNe whose hosts are radio-detected are not plotted. Same source with different observing epochs is connected with a solid line.

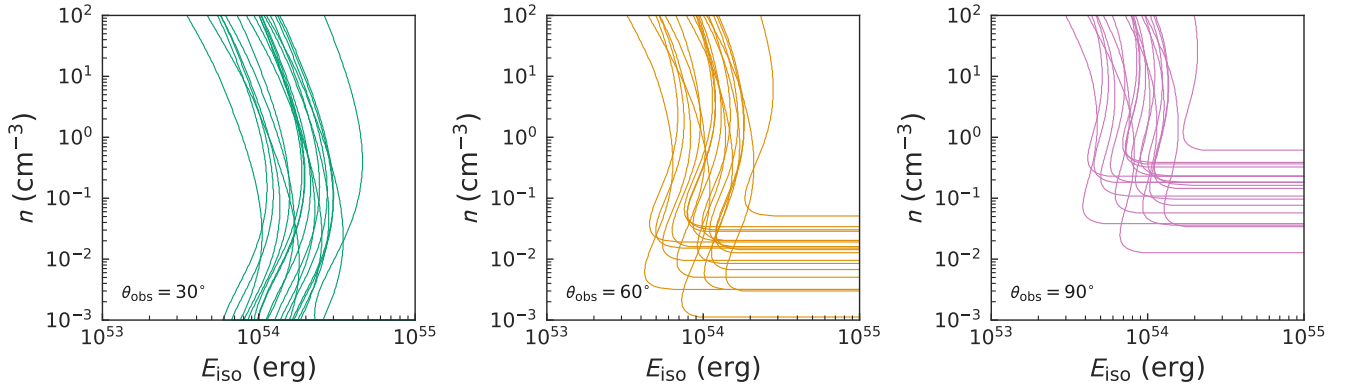


Figure 7. Pairs of isotropic equivalent energies (E_{iso}) and CSM densities (n) which reach the observed 3 GHz flux density (or upper upper limit) for each SLSN calculated with the `afterglowpy` code (Ryan et al. 2020) with viewing angles of $\theta_{\text{obs}} = 30^\circ$, 60° , and 90° . A lower left (lower energy and density) region of each line represents the allow parameters for each SLSN.

Table 6. Score sheet for magnetar wind nebular models constrained by this study

SLSN	with absorption		without absorption	
Model of Omand et al. (2018)				
	P_{\min}	P_{\max}	P_{\min}	P_{\max}
SN 2011ke	Excluded	Excluded	Excluded	Excluded
SN 2012il	Excluded	Excluded	Excluded	Excluded
Model of Law et al. (2019)				
	P_{\min}	P_{\max}	P_{\min}	P_{\max}
PTF09cnd		Excluded		Excluded
SN 2007bi		Excluded	Excluded	Excluded
SN 2010kd		Excluded		Excluded
SN 2011ke	Excluded	Excluded	Excluded	Excluded
Model of Eftekhari et al. (2021)				
PTF09cnd				Excluded
SN 2007bi	Excluded			Excluded

time radio data. We detected radio emission in six sources (PTF10hgi, PTF10qaf, PTF10uhf, PTF12dam, SN 1999bd, SN 2006gy) with $S/N > 5$, and tentatively detected in two sources (SN 2007bw and SN 2012il) with $S/N \sim 3.6$. The key findings are as follows:

1. The radio-detected sources were observed more than once, and we examined the time variability. No significant variability was found in the $>5\sigma$ sources except for PTF10hgi, which was reported to have a variability in the literature. This suggests that the emission arise from activity in the hosts for PTF10qaf, PTF10uhf, PTF12dam, SN 1999bd, and SN 2006gy, coupled with the fact that the radio peak positions are consistent with the galaxy centers.
2. We compared SFRs derived from the 3 GHz flux densities with SFRs from the SED modelling based on rest-frame UV to NIR data. We found that four hosts (PTF10qaf, PTF10uhf, PTF12dam, and SN 1999bd) have an excess of radio-based SFRs over SED-based SFRs, suggesting that there exists obscured star formation that cannot be traced by UV–NIR data. The obscured star formation is consistent with their starburst nature and/or large stellar masses. The upper limits for the undetected hosts and stacked results show that the majority of the SLSN hosts do not have a significant obscured star formation.
3. We compared radio-based SFRs and stellar masses and found that the hosts of PTF10qaf and

PTF12dam are located above the galaxy main sequence, the hosts of SN 1999bd and PTF10uhf are within the range of the main sequence, and the SN 2006gy host is below the main sequence. Our results are consistent overall with the fact that the hosts of SLSNe have higher sSFR compared to main-sequence galaxies reported in the literature, but are not stringent because of the limited sensitivity of the radio observations.

4. By using our 3 GHz radio upper limits, we constrained the parameters for afterglows arising from off-axis jets. We found that the radio upper limits excluded the models with a higher energy ($E_{\text{iso}} \gtrsim \text{several} \times 10^{53}$ erg) and higher CSM densities ($n \gtrsim 0.01 \text{ cm}^{-3}$), but lower energies or lower CSM densities were not excluded with the current data.
5. We constrained the models of electron–positron PWNe caused by pulsar/magnetar-driven SLSNe by comparing the 3 GHz upper limits with the predictions in the literature. The models for some of the SLSNe in our sample (PTF09cnd, SN 2007bi, SN 2010kd, SN 2011ke, SN 2012il, and SN 2015bn) were constrained, but the predictions for the remaining SLSNe-I were not ruled out in the current data.

So far, about 30 SLSNe were observed in radio and only a few SLSNe had radio detections. In addition, the current sensitivity is insufficient to constrain parameters of models for SLSNe or obscured star formation in their hosts. High-sensitivity, long-term monitoring observations of a large sample will allow us to examine the physical nature of SLSNe. Observations with future radio telescopes such as the Square Kilometer Array (SKA)³ and the Next Generation VLA (ngVLA)⁴ will open a new window toward understanding extreme transient events.

We thank the referee for helpful comments and suggestions which significantly improved the paper. We are grateful to Masao Hayashi and the PDJ collaboration for fruitful discussions. We would like to acknowledge NRAO staffs for their help in preparation of observations. BH is supported by JSPS KAKENHI Grant Number 19K03925.

The National Radio Astronomy Observatory is a facility of the National Science Foundation operated under cooperative agreement by Associated Universities, Inc.

³ <https://www.skatelescope.org/>

⁴ <https://ngvla.nrao.edu/>

Based on observations made with the NASA/ESA Hubble Space Telescope, and obtained from the Hubble Legacy Archive, which is a collaboration between the Space Telescope Science Institute (STScI/NASA), the Space Telescope European Coordinating Facility (ST-ECF/ESA) and the Canadian Astronomy Data Centre (CADC/NRC/CSA).

This project used public archival data from the Dark Energy Survey (DES). Funding for the DES Projects has been provided by the U.S. Department of Energy, the U.S. National Science Foundation, the Ministry of Science and Education of Spain, the Science and Technology Facilities Council of the United Kingdom, the Higher Education Funding Council for England, the National Center for Supercomputing Applications at the University of Illinois at Urbana-Champaign, the Kavli Institute of Cosmological Physics at the University of Chicago, the Center for Cosmology and Astro-Particle Physics at the Ohio State University, the Mitchell Institute for Fundamental Physics and Astronomy at Texas A&M University, Financiadora de Estudos e Projetos, Fundação Carlos Chagas Filho de Amparo à Pesquisa do Estado do Rio de Janeiro, Conselho Nacional de Desenvolvimento Científico e Tecnológico and the Ministério da Ciência, Tecnologia e Inovação, the Deutsche Forschungsgemeinschaft, and the Collaborating Institutions in the Dark Energy Survey.

The Collaborating Institutions are Argonne National Laboratory, the University of California at Santa Cruz,

the University of Cambridge, Centro de Investigaciones Energéticas, Medioambientales y Tecnológicas-Madrid, the University of Chicago, University College London, the DES-Brazil Consortium, the University of Edinburgh, the Eidgenössische Technische Hochschule (ETH) Zürich, Fermi National Accelerator Laboratory, the University of Illinois at Urbana-Champaign, the Institut de Ciències de l’Espai (IEEC/CSIC), the Institut de Física d’Altes Energies, Lawrence Berkeley National Laboratory, the Ludwig-Maximilians Universität München and the associated Excellence Cluster Universe, the University of Michigan, the National Optical Astronomy Observatory, the University of Nottingham, The Ohio State University, the OzDES Membership Consortium, the University of Pennsylvania, the University of Portsmouth, SLAC National Accelerator Laboratory, Stanford University, the University of Sussex, and Texas A&M University.

Based in part on observations at Cerro Tololo Inter-American Observatory, National Optical Astronomy Observatory, which is operated by the Association of Universities for Research in Astronomy (AURA) under a cooperative agreement with the National Science Foundation.

Facility: Karl G. Jansky Very Large Array

Software: CASA (McMullin et al. 2007), *afterglowpy* (Ryan et al. 2020), *ASTROPY* (Robitaille et al. 2013; Price-Whelan et al. 2018), *MATPLOTLIB* (Hunter 2007)

REFERENCES

- Abbott, T. M. C., Abdalla, F. B., Allam, S., et al. 2018, *The Astrophysical Journal Supplement Series*, 239, 18, doi: [10.3847/1538-4365/aae9f0](https://doi.org/10.3847/1538-4365/aae9f0)
- Alexander, K. D., Nicholl, M., Berger, E., & Margutti, R. 2016, *The Astronomer’s Telegram*, 8552
- Andersen, B. C., Bandura, K. M., Bhardwaj, M., et al. 2020, *Nature*, 587, 54, doi: [10.1038/s41586-020-2863-y](https://doi.org/10.1038/s41586-020-2863-y)
- Angus, C. R., Levan, A. J., Perley, D. A., et al. 2016, *Monthly Notices of the Royal Astronomical Society*, 458, 84, doi: [10.1093/mnras/stw063](https://doi.org/10.1093/mnras/stw063)
- Arabsalmani, M., Roychowdhury, S., Renaud, F., et al. 2019, *The Astrophysical Journal*, 882, 31, doi: [10.3847/1538-4357/ab2897](https://doi.org/10.3847/1538-4357/ab2897)
- Baldwin, J. A., Phillips, M. M., & Terlevich, R. 1981, *Publications of the Astronomical Society of the Pacific*, 93, 5, doi: [10.1086/130766](https://doi.org/10.1086/130766)
- Becker, R. H., White, R. L., & Helfand, D. J. 1995, *The Astrophysical Journal*, 450, 559, doi: [10.1086/176166](https://doi.org/10.1086/176166)
- Bochenek, C. D., Ravi, V., Belov, K. V., et al. 2020, *Nature*, 587, 59, doi: [10.1038/s41586-020-2872-x](https://doi.org/10.1038/s41586-020-2872-x)
- Bock, D. C.-J., Large, M. I., & Sadler, E. M. 1999, *The Astronomical Journal*, 117, 1578, doi: [10.1086/300786](https://doi.org/10.1086/300786)
- Bose, S., Dong, S., Pastorello, A., et al. 2018, *The Astrophysical Journal*, 853, 57, doi: [10.3847/1538-4357/aaa298](https://doi.org/10.3847/1538-4357/aaa298)
- Chabrier, G. 2003, *Publications of the Astronomical Society of the Pacific*, 115, 763, doi: [10.1086/376392](https://doi.org/10.1086/376392)
- Chandra, P., Ofek, E. O., Frail, D. A., et al. 2009, *The Astronomer’s Telegram*, 2241
- . 2010, *The Astronomer’s Telegram*, 2367
- Chen, B.-Q., Liu, X.-W., Yuan, H.-B., Huang, Y., & Xiang, M.-S. 2015, *Monthly Notices of the Royal Astronomical Society*, 448, 2187, doi: [10.1093/mnras/stv103](https://doi.org/10.1093/mnras/stv103)
- Chen, T.-W., Nicholl, M., Smartt, S. J., et al. 2017, *Astronomy & Astrophysics*, 602, A9, doi: [10.1051/0004-6361/201630163](https://doi.org/10.1051/0004-6361/201630163)

- Chevalier, R. A., & Irwin, C. M. 2011, *The Astrophysical Journal*, 729, L6, doi: [10.1088/2041-8205/729/1/L6](https://doi.org/10.1088/2041-8205/729/1/L6)
- Chomiuk, L., Soderberg, A., Margutti, R., et al. 2012, *The Astronomer's Telegram*, 3931
- Condon, J. J. 1992, *Annual Review of Astronomy and Astrophysics*, 30, 575, doi: [10.1146/annurev.aa.30.090192.003043](https://doi.org/10.1146/annurev.aa.30.090192.003043)
- Condon, J. J., Cotton, W. D., Greisen, E. W., et al. 1998, *The Astronomical Journal*, 115, 1693, doi: [10.1086/300337](https://doi.org/10.1086/300337)
- Cooke, J., Sullivan, M., Gal-Yam, A., et al. 2012, *Nature*, 491, 228, doi: [10.1038/nature11521](https://doi.org/10.1038/nature11521)
- Coppejans, D. L., Margutti, R., Guidorzi, C., et al. 2018, *The Astrophysical Journal*, 856, 56, doi: [10.3847/1538-4357/aab36e](https://doi.org/10.3847/1538-4357/aab36e)
- Cordes, J. M., & Chatterjee, S. 2019, *Annual Review of Astronomy and Astrophysics*, 57, 417, doi: [10.1146/annurev-astro-091918-104501](https://doi.org/10.1146/annurev-astro-091918-104501)
- Delhaize, J., Smolčić, V., Delvecchio, I., et al. 2017, *Astronomy and Astrophysics*, 602, A4, doi: [10.1051/0004-6361/201629430](https://doi.org/10.1051/0004-6361/201629430)
- Dexter, J., & Kasen, D. 2013, *The Astrophysical Journal*, 772, 30, doi: [10.1088/0004-637X/772/1/30](https://doi.org/10.1088/0004-637X/772/1/30)
- Eftekhari, T., Berger, E., Margalit, B., Metzger, B. D., & Williams, P. K. G. 2020, *The Astrophysical Journal*, 895, 98, doi: [10.3847/1538-4357/ab9015](https://doi.org/10.3847/1538-4357/ab9015)
- Eftekhari, T., Berger, E., Margalit, B., et al. 2019, *The Astrophysical Journal*, 876, L10, doi: [10.3847/2041-8213/ab18a5](https://doi.org/10.3847/2041-8213/ab18a5)
- Eftekhari, T., Margalit, B., Omand, C. M. B., et al. 2021, *The Astrophysical Journal*, 912, 21, doi: [10.3847/1538-4357/abe9b8](https://doi.org/10.3847/1538-4357/abe9b8)
- Elbaz, D., Dickinson, M., Hwang, H. S., et al. 2011, *Astronomy & Astrophysics*, 533, A119, doi: [10.1051/0004-6361/201117239](https://doi.org/10.1051/0004-6361/201117239)
- Flaugher, B., Diehl, H. T., Honscheid, K., et al. 2015, *The Astronomical Journal*, 150, 150, doi: [10.1088/0004-6256/150/5/150](https://doi.org/10.1088/0004-6256/150/5/150)
- Gal-Yam, A. 2012, *Science*, 337, 927, doi: [10.1126/science.1203601](https://doi.org/10.1126/science.1203601)
- . 2019, *Annual Review of Astronomy and Astrophysics*, 57, 305, doi: [10.1146/annurev-astro-081817-051819](https://doi.org/10.1146/annurev-astro-081817-051819)
- Guillochon, J., Parrent, J., Kelley, L. Z., & Margutti, R. 2017, *The Astrophysical Journal*, 835, 64, doi: [10.3847/1538-4357/835/1/64](https://doi.org/10.3847/1538-4357/835/1/64)
- Hatsukade, B., Tominaga, N., Hayashi, M., et al. 2018, *The Astrophysical Journal*, 857, 72, doi: [10.3847/1538-4357/aab616](https://doi.org/10.3847/1538-4357/aab616)
- Hatsukade, B., Morokuma-Matsui, K., Hayashi, M., et al. 2020, *Publications of the Astronomical Society of Japan*, 72, L6, doi: [10.1093/pasj/psaa052](https://doi.org/10.1093/pasj/psaa052)
- Hatsukade, B., Tominaga, N., Morokuma, T., et al. 2021, *The Astrophysical Journal Letters*, 911, L1, doi: [10.3847/2041-8213/abef03](https://doi.org/10.3847/2041-8213/abef03)
- Hunter, J. D. 2007, *Computing in Science Engineering*, 9, 90, doi: [10.1109/MCSE.2007.55](https://doi.org/10.1109/MCSE.2007.55)
- Jiménez-Andrade, E. F., Murphy, E. J., Heywood, I., et al. 2021, *The Astrophysical Journal*, 910, 106, doi: [10.3847/1538-4357/abe876](https://doi.org/10.3847/1538-4357/abe876)
- Kasen, D., & Bildsten, L. 2010, *The Astrophysical Journal*, 717, 245, doi: [10.1088/0004-637X/717/1/245](https://doi.org/10.1088/0004-637X/717/1/245)
- Kashiyama, K., & Murase, K. 2017, *The Astrophysical Journal*, 839, L3, doi: [10.3847/2041-8213/aa68e1](https://doi.org/10.3847/2041-8213/aa68e1)
- Law, C. J., Omand, C. M. B., Kashiyama, K., et al. 2019, *The Astrophysical Journal*, 886, 24, doi: [10.3847/1538-4357/ab4adb](https://doi.org/10.3847/1538-4357/ab4adb)
- Leloudas, G., Hsiao, E. Y., Johansson, J., et al. 2015a, *Astronomy & Astrophysics*, 574, A61, doi: [10.1051/0004-6361/201322035](https://doi.org/10.1051/0004-6361/201322035)
- Leloudas, G., Schulze, S., Krühler, T., et al. 2015b, *Monthly Notices of the Royal Astronomical Society*, 449, 917, doi: [10.1093/mnras/stv320](https://doi.org/10.1093/mnras/stv320)
- Lunnan, R., Chornock, R., Berger, E., et al. 2014, *The Astrophysical Journal*, 787, 138, doi: [10.1088/0004-637X/787/2/138](https://doi.org/10.1088/0004-637X/787/2/138)
- Margalit, B., & Metzger, B. D. 2018, *The Astrophysical Journal Letters*, 868, L4, doi: [10.3847/2041-8213/aaedad](https://doi.org/10.3847/2041-8213/aaedad)
- Margalit, B., Metzger, B. D., Berger, E., et al. 2018a, *Monthly Notices of the Royal Astronomical Society*, 481, 2407, doi: [10.1093/mnras/sty2417](https://doi.org/10.1093/mnras/sty2417)
- Margalit, B., Metzger, B. D., Thompson, T. A., Nicholl, M., & Sukhbold, T. 2018b, *Monthly Notices of the Royal Astronomical Society*, 475, 2659, doi: [10.1093/mnras/sty013](https://doi.org/10.1093/mnras/sty013)
- McMullin, J. P., Waters, B., Schiebel, D., Young, W., & Golap, K. 2007, 376, 127
- Metzger, B. D., Berger, E., & Margalit, B. 2017, *The Astrophysical Journal*, 841, 14, doi: [10.3847/1538-4357/aa633d](https://doi.org/10.3847/1538-4357/aa633d)
- Metzger, B. D., & Bower, G. C. 2014, *Monthly Notices of the Royal Astronomical Society*, 437, 1821, doi: [10.1093/mnras/stt2010](https://doi.org/10.1093/mnras/stt2010)
- Metzger, B. D., Margalit, B., Kasen, D., & Quataert, E. 2015, *Monthly Notices of the Royal Astronomical Society*, 454, 3311, doi: [10.1093/mnras/stv2224](https://doi.org/10.1093/mnras/stv2224)
- Meusinger, H., Brunsendorf, J., & Krieg, R. 2000, *Astronomy and Astrophysics*, 363, 933

- Mondal, S., Bera, A., Chandra, P., & Das, B. 2020, *Monthly Notices of the Royal Astronomical Society*, 498, 3863, doi: [10.1093/mnras/staa2637](https://doi.org/10.1093/mnras/staa2637)
- Morganson, E., Gruendl, R. A., Menanteau, F., et al. 2018, *Publications of the Astronomical Society of the Pacific*, 130, 074501, doi: [10.1088/1538-3873/aab4ef](https://doi.org/10.1088/1538-3873/aab4ef)
- Moriya, T. J., Sorokina, E. I., & Chevalier, R. A. 2018, *Space Science Reviews*, 214, 59, doi: [10.1007/s11214-018-0493-6](https://doi.org/10.1007/s11214-018-0493-6)
- Moriya, T. J., Tanaka, M., Yasuda, N., et al. 2019, *The Astrophysical Journal Supplement Series*, 241, 16, doi: [10.3847/1538-4365/ab07c5](https://doi.org/10.3847/1538-4365/ab07c5)
- Murase, K., Kashiyama, K., Kiuchi, K., & Bartos, I. 2015, *The Astrophysical Journal*, 805, 82, doi: [10.1088/0004-637X/805/1/82](https://doi.org/10.1088/0004-637X/805/1/82)
- Murase, K., Kashiyama, K., & Mészáros, P. 2016, *Monthly Notices of the Royal Astronomical Society*, 461, 1498, doi: [10.1093/mnras/stw1328](https://doi.org/10.1093/mnras/stw1328)
- Murase, K., Omand, C. M. B., Coppejans, D. L., et al. 2021, arXiv:2105.05239
- Murphy, E. J., Momjian, E., Condon, J. J., et al. 2017, *The Astrophysical Journal*, 839, 35, doi: [10.3847/1538-4357/aa62fd](https://doi.org/10.3847/1538-4357/aa62fd)
- Murphy, E. J., Condon, J. J., Schinnerer, E., et al. 2011, *The Astrophysical Journal*, 737, 67, doi: [10.1088/0004-637X/737/2/67](https://doi.org/10.1088/0004-637X/737/2/67)
- Murphy, E. J., Bremseth, J., Mason, B. S., et al. 2012, *The Astrophysical Journal*, 761, 97, doi: [10.1088/0004-637X/761/2/97](https://doi.org/10.1088/0004-637X/761/2/97)
- Nicholl, M., Berger, E., Smartt, S. J., et al. 2016, *The Astrophysical Journal*, 826, 39, doi: [10.3847/0004-637X/826/1/39](https://doi.org/10.3847/0004-637X/826/1/39)
- Nicholl, M., Blanchard, P. K., Berger, E., et al. 2018, *The Astrophysical Journal*, 866, L24, doi: [10.3847/2041-8213/aae70d](https://doi.org/10.3847/2041-8213/aae70d)
- Omand, C. M. B., Kashiyama, K., & Murase, K. 2018, *Monthly Notices of the Royal Astronomical Society*, 474, 573, doi: [10.1093/mnras/stx2743](https://doi.org/10.1093/mnras/stx2743)
- Perley, D. A., Quimby, R. M., Yan, L., et al. 2016, *The Astrophysical Journal*, 830, 13, doi: [10.3847/0004-637X/830/1/13](https://doi.org/10.3847/0004-637X/830/1/13)
- Perley, R. A., & Butler, B. J. 2017, *The Astrophysical Journal Supplement Series*, 230, 7, doi: [10.3847/1538-4365/aa6df9](https://doi.org/10.3847/1538-4365/aa6df9)
- Planck Collaboration, Aghanim, N., Akrami, Y., et al. 2020, *Astronomy and Astrophysics*, 641, A6, doi: [10.1051/0004-6361/201833910](https://doi.org/10.1051/0004-6361/201833910)
- Price-Whelan, a. A. M., Sip\Hocz, B. M., Günther, H. M., et al. 2018, *The Astrophysical Journal*, 156, 123, doi: [10.3847/1538-3881/aabc4f](https://doi.org/10.3847/1538-3881/aabc4f)
- Robitaille, T. P., Tollerud, E. J., Greenfield, P., et al. 2013, *Astronomy & Astrophysics*, 558, A33, doi: [10.1051/0004-6361/201322068](https://doi.org/10.1051/0004-6361/201322068)
- Rodighiero, G., Daddi, E., Baronchelli, I., et al. 2011, *The Astrophysical Journal*, 739, L40, doi: [10.1088/2041-8205/739/2/L40](https://doi.org/10.1088/2041-8205/739/2/L40)
- Ryan, G., van Eerten, H., Piro, L., & Troja, E. 2020, *The Astrophysical Journal*, 896, 166, doi: [10.3847/1538-4357/ab93cf](https://doi.org/10.3847/1538-4357/ab93cf)
- Schreiber, C., Pannella, M., Elbaz, D., et al. 2015, *Astronomy & Astrophysics*, 575, A74, doi: [10.1051/0004-6361/201425017](https://doi.org/10.1051/0004-6361/201425017)
- Schulze, S., Krühler, T., Leloudas, G., et al. 2018, *Monthly Notices of the Royal Astronomical Society*, 473, 1258, doi: [10.1093/mnras/stx2352](https://doi.org/10.1093/mnras/stx2352)
- Smith, N., & McCray, R. 2007, *The Astrophysical Journal*, 671, L17, doi: [10.1086/524681](https://doi.org/10.1086/524681)
- Smith, N., Li, W., Foley, R. J., et al. 2007, *The Astrophysical Journal*, 666, 1116, doi: [10.1086/519949](https://doi.org/10.1086/519949)
- Smolčić, V., Miettinen, O., Tomičić, N., et al. 2017a, *Astronomy and Astrophysics*, 597, A4, doi: [10.1051/0004-6361/201526989](https://doi.org/10.1051/0004-6361/201526989)
- Smolčić, V., Delvecchio, I., Zamorani, G., et al. 2017b, *Astronomy & Astrophysics*, 602, A2, doi: [10.1051/0004-6361/201630223](https://doi.org/10.1051/0004-6361/201630223)
- Taggart, K., & Perley, D. A. 2021, *Monthly Notices of the Royal Astronomical Society*, 503, 3931, doi: [10.1093/mnras/stab174](https://doi.org/10.1093/mnras/stab174)
- Thöne, C. C., de Ugarte Postigo, A., García-Benito, R., et al. 2015, *Monthly Notices of the Royal Astronomical Society: Letters*, 451, L65, doi: [10.1093/mnrasl/slv051](https://doi.org/10.1093/mnrasl/slv051)
- van Eerten, H., van der Horst, A., & MacFadyen, A. 2012, *The Astrophysical Journal*, 749, 44, doi: [10.1088/0004-637X/749/1/44](https://doi.org/10.1088/0004-637X/749/1/44)
- Wang, X.-G., Zhang, B., Liang, E.-W., et al. 2015, *The Astrophysical Journal Supplement Series*, 219, 9, doi: [10.1088/0067-0049/219/1/9](https://doi.org/10.1088/0067-0049/219/1/9)
- Whitaker, K. E., Pope, A., Cybulski, R., et al. 2017, *The Astrophysical Journal*, 850, 208, doi: [10.3847/1538-4357/aa94ce](https://doi.org/10.3847/1538-4357/aa94ce)
- Woolsey, S. E. 2010, *The Astrophysical Journal*, 719, L204, doi: [10.1088/2041-8205/719/2/L204](https://doi.org/10.1088/2041-8205/719/2/L204)
- Woolsey, S. E., Blinnikov, S., & Heger, A. 2007, *Nature*, 450, 390, doi: [10.1038/nature06333](https://doi.org/10.1038/nature06333)